ACS Catalysis

Research Article

Cite This: ACS Catal. 2020, 10, 751−761

pubs.acs.org/acscatalysis

Host−Guest Chemistry Meets Electrocatalysis: Cucurbit[6]uril on a Au Surface as a Hybrid System in CO_2 Reduction

Andreas Wagner,[†,○] Khoa H. Ly,[†,○,◆] Nina Heidary,[†,¶] István Szabó,[§] Tamás Földes,[§] Khaleel I. Assaf,[∥,□] Steven J. Barrow,[‡,&] Kamil Sokołowski,[‡,⊥] Mohamed Al-Hada,[#] Nikolay Kornienko,[†,¶] Moritz F. Kuehnel,[†,●] Edina Rosta,[§] Ingo Zebger,[▽] Werner M. Nau,[∥] Oren A. Scherman,*[,‡] and Erwin Reisner*[,†]

[†]Christian Doppler Laboratory for Sustainable SynGas Chemistry, Department of Chemistry and [‡]Melville Laboratory for Polymer Synthesis, Department of Chemistry, University of Cambridge, Lensfield Road, Cambridge CB2 1EW, United Kingdom

[§]Department of Chemistry, King's College London, 7 Trinity Street, SE1 1DB London, United Kingdom

[∥]Department of Life Sciences and Chemistry, Jacobs University Bremen, Campus Ring 1, 28759 Bremen, Germany

[⊥]Institute of Physical Chemistry, Polish Academy of Sciences, Kasprzaka 44/52, 01-224 Warsaw, Poland

[#]Cavendish Laboratory, Department of Physics, University of Cambridge, JJ Thomson Ave, Cambridge CB3 0HE, United Kingdom

[▽]Max Volmer Laboratorium für Biophysikalische Chemie, Sekr. PC14, Institut für Chemie, Technische Universität Berlin, Straße des 17. Juni 135, 10623 Berlin, Germany

Supporting Information

ABSTRACT: The rational control of forming and stabilizing reaction intermediates to guide specific reaction pathways remains to be a major challenge in electrocatalysis. In this work, we report a surface active-site engineering approach for modulating electrocatalytic CO_2 reduction using the macrocycle cucurbit[6]uril (CB[6]). A pristine gold surface functionalized with CB[6] nanocavities was studied as a hybrid organic−inorganic model system that utilizes host−guest chemistry to influence the heterogeneous electrocatalytic reaction. The combination of surface-enhanced infrared absorption (SEIRA) spectroscopy and electrocatalytic experiments in conjunction with theoretical calculations supports capture and reduction of CO_2 inside the hydrophobic cavity of CB[6] on the gold surface in aqueous $KHCO_3$ at negative potentials. SEIRA spectroscopic experiments show that the decoration of gold with the supramolecular host CB[6] leads to an increased local CO_2 concentration close to the metal interface. Electrocatalytic CO_2 reduction on a CB[6]-coated gold electrode indicates differences in the specific interactions between CO_2 reduction intermediates within and outside the CB[6] molecular cavity, illustrated by a decrease in current density from CO generation, but almost invariant H_2 production compared to unfunctionalized gold. The presented methodology and mechanistic insight can guide future design of molecularly engineered catalytic environments through interfacial host−guest chemistry.

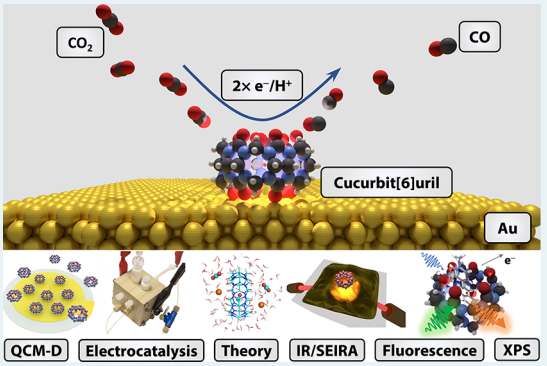

KEYWORDS: *surface active-site engineering, electrocatalytic CO_2 reduction, host−guest chemistry, supramolecular catalysis*

INTRODUCTION

The electrocatalytic reduction of CO_2 using renewable energy sources offers an attractive route to produce storable carbon-neutral fuels.[1,2] For this technology to become commercially viable, catalysts that promote the challenging multi-electron/-proton transfer reaction with minimal energy losses and high rate and selectivity need to be developed. Currently, CO_2 reduction suffers from significant overpotentials, sluggish kinetics, and low selectivity control as well as the low solubility of CO_2 in aqueous electrolytes.[3−5] Gold (Au) is generally considered the most active electrocatalyst for CO generation with a catalytic onset potential ca. 300 mV more negative than the standard potential for CO_2 to CO reduction on flat electrodes.[6−8] The catalytic mechanism on Au is believed to involve a surface-bound COOH (*COOH) intermediate, which is subsequently further reduced by 1 e^-/1 H^+ transfer to yield CO (*CO) that is finally liberated from the surface. Theoretical predictions indicate that stronger binding of the *COOH intermediate relative to *CO may be needed for enhanced CO evolution activity.[9,10] However, the binding energies of *COOH and *CO on electrocatalysts generally correlate;[11] therefore, stabilization of *COOH would simultaneously stabilize *CO and thus disfavor its required desorption. This scaling relationship impedes a straightforward

Received: September 30, 2019
Revised: November 18, 2019
Published: November 20, 2019

DOI: 10.1021/acscatal.9b04221
ACS Catal. 2020, 10, 751−761

approach to independently fine-tune surface properties for higher activities, hampering the development of low overpotential single-site metal catalysts.[12]

To this end, different approaches such as alloying,[13,14] nanostructuring,[15] and molecular surface modification[16−20] have recently gained attention. Nevertheless, molecular engineering of an electrocatalytic surface site remains to be challenging. Nature, on the other hand, has developed very effective catalytic systems that surpass the limits of scaling relationships. Enzymes such as carbon monoxide dehydrogenase and formate dehydrogenase are able to reversibly interconvert CO_2 at the thermodynamic potential with quantitative product selectivity at their precious-metal free active sites.[21−23] While details about their reaction mechanisms are still under debate, a hydrophobic active site cavity and the stabilization of intermediates by a highly specific second coordination sphere are believed to be crucial for their high activity as well as selectivity.[9,24,25]

In our efforts to create analogous synthetic reaction environments, we envision supramolecular host−guest chemistry as a powerful tool to modulate electrocatalytic reactions by selectively favoring certain species due to highly specific binding affinities. Cucurbit[*n*]urils (CB[*n*] where $n = 5−8$) are a class of promising host molecules for this purpose. These barrel-shaped organic macrocycles are water-soluble and have found broad applications in materials chemistry, drug delivery systems, sensing, and catalysis (Figure 1a).[26,27] CB[*n*]s are able to shift the reduction potential of electrochemical processes by selectively stabilizing certain species.[28,29] For example, half-wave potentials of ferrocene and methyl viologen can be positively shifted upon complexation with CB[7] due to different stabilization of the oxidized versus reduced species within the cavity.

The cavities of CB[*n*] are highly hydrophobic[30] and bind a plethora of small organic guests (for $n \geq 6$) as well as gas molecules (for $n \leq 6$).[26] In aqueous solutions, a large number of gases (e.g., CH_4, acetylene, and cyclopentane) form inclusion complexes within CB[6].[31] Their negatively polarized carbonyl-lined portals exhibit high affinity toward metal surfaces allowing for facile supramolecular functionalization of electrodes.[32] In contrast, other hosts such as pillararenes, cyclodextrins, and calixarenes typically rely on additional steps for electrode immobilization, which often afford increased distances between the host cavity and the surface.[33−35] Their ability to directly affect surface-bound species is thereby diminished.

It has been shown spectroscopically and by gravimetric measurements that CB[6] can be used as a highly porous solid-state adsorbent for gaseous CO_2 with high selectivity over CO,

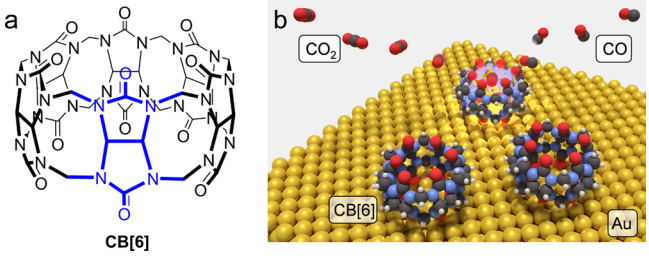

Figure 1. (a) CB[6] structure with monomeric building block highlighted in blue. (b) Schematic illustration of CO_2 conversion to CO within the cavity of CB[6] adsorbed on a Au surface.

rendering this molecule to be attractive for combining host−guest chemistry and electrocatalytic CO_2 reduction studies.[36,37] To the best of our knowledge, neither has CO_2 complexation within CB[6] in solution been demonstrated nor has CB[6] been used in electrocatalytic CO_2 reduction.

In this work, we study CB[6] as a prototypical synthetic organic cavity system for facile manipulation of the heterogeneous CO_2 reduction on Au, a well-studied model electrocatalyst (Figure 1b). First, the host−guest interaction of CO_2 with CB[6] is studied in homogeneous aqueous solution both experimentally and computationally. Subsequently, we employ surface-enhanced infrared absorption (SEIRA) spectroscopy combined with electrochemistry to investigate the behavior of CO_2 within CB[6] on the Au surface during electrocatalysis.

RESULTS AND DISCUSSION

Interaction of CO_2 with CB[6] in Solution. The inclusion of CO_2 in CB[6] was monitored in aqueous $KHCO_3$ (0.1 M) using Fourier-transform infrared (FTIR) spectroscopy in transmission mode (Figure 2a). The asymmetric stretching mode of $^{12}CO_2$ was found at 2343 cm^{-1}, which is in line with previously reported values for $^{12}CO_2$ in solution.[38] In the presence of 8.44 mM CB[6], an additional shoulder was detected at 2333 cm^{-1}. This band was exclusively observed in a $^{12}CO_2$-purged electrolyte solution (Figure S1) and therefore assigned to an interaction between CO_2 and CB[6] (CB[6]·CO_2). The corresponding $^{13}CO_2$ asymmetric stretching vibration[38] identified at 2278 cm^{-1} displayed an identical shift by 10 cm^{-1} to 2268 cm^{-1}, confirming this band to originate from CO_2.

The observed shift matches the previously reported values for the asymmetric stretching mode of CO_2 confined in solid CB[6] at 2336 cm^{-1}.[36,37] Addition of spermine, a well-known CB[6] guest with a high binding affinity,[26] led to disappearance of the band at 2333 cm^{-1}, which is in line with a competitive displacement of CO_2 from the cavity. Moreover, the IR signature of the CB[6] framework remained unchanged in the presence of N_2 and $^{12}CO_2/^{13}CO_2$, indicating that the CB[6]·CO_2 (binding) interaction is weak and nondirectional (Figure 2b). In contrast, spermine addition gave rise to a strong additional band at 1727 cm^{-1}. This band can be rationalized by a shift of the carbonyl stretching mode from 1743 cm^{-1} by 16 cm^{-1} as a result of electrostatic interactions with the positively charged amine functional group of spermine.[39] Analogously, the unaltered CB[6] carbonyl band in the presence of CO_2, when compared to the CB[6]·spermine host−guest complex, suggests that CO_2 is not merely associated with the carbonyl portal region of CB[6]. In conclusion, the IR data strongly suggests that CO_2 is bound inside the CB[6] cavity in solution with an IR marker band located at 2333 cm^{-1}. We note that the binding of CO to CB[6] could not be probed due to its low solubility in the reaction solution.

The assignment of the CO_2 interaction with CB[6] is further corroborated by density functional theory (DFT) and molecular dynamics (MD) simulations (Table S1 and Figures S2−S5). Both methods show a stronger binding of CO_2 over CO in CB[6], which is in line with previously reported DFT results.[40] A free-energy profile based on umbrella sampling of MD simulations of CO_2 and CO is shown in Figure 3a. The results suggest that CO_2 and CO need to overcome a low energy barrier when entering the cavity and reach an energy

DOI: 10.1021/acscatal.9b04221
ACS Catal. 2020, 10, 751−761

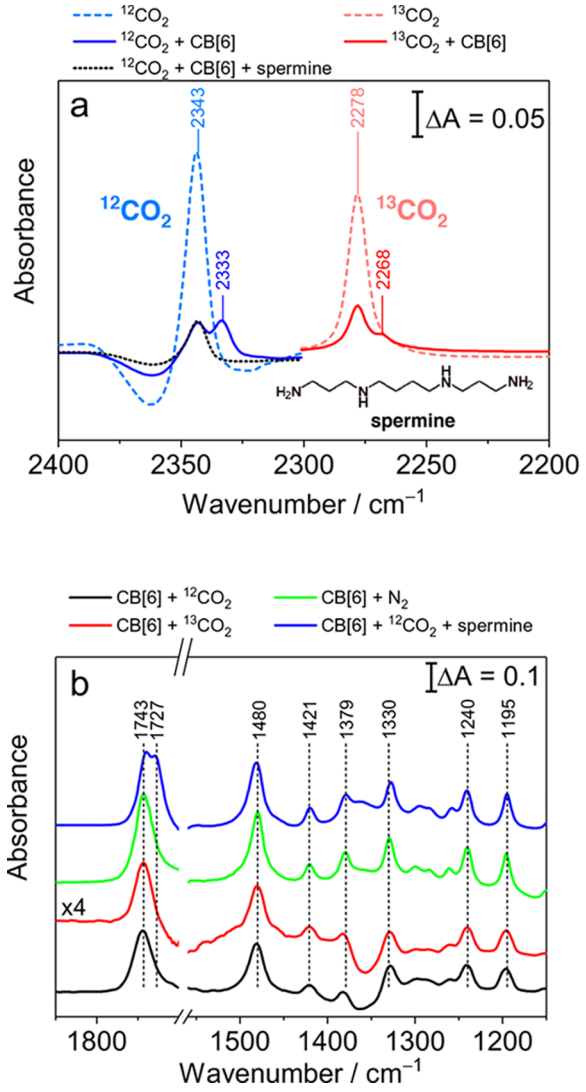

Figure 2. FTIR spectra of CB[6] solutions recorded in the transmission mode. (a) Absorbance spectra of asymmetric stretching modes of $^{12}CO_2$ in aqueous $KH^{12}CO_3$ (0.1 M) and $^{13}CO_2$ in $NaH^{13}CO_3$ (0.1 M) solution. The reference spectra for dashed spectra were the N_2 purged electrolytes. Spectra of CB[6] from which the CB-free CO_2 reference spectrum was subtracted display a shoulder at 2333 and 2268 cm^{-1}. The addition of spermine (strong CB[6] cavity binder) leads to disappearance of the 2333 cm^{-1} band. The broad negative band at ca. 2360 cm^{-1} results from small atmospheric CO_2 variations between measurements. (b) IR spectra of the region below 1800 cm^{-1} representing the vibrational modes for CB[6] in $^{12}CO_2$-purged 0.1 M $KH^{12}CO_3$ and $^{13}CO_2$-purged 0.1 M $NaH^{13}CO_3$, which exhibit no band shifts in comparison to the N_2-purged 0.1 M $KH^{12}CO_3$ solution. Addition of spermine leads to an additional band at 1727 cm^{-1} assigned to carbonyl functional groups of CB[6], presumably occurring due to the interaction of the spermine nitrogen and CB[6] carbonyl ring. The spectrum of the CB[6] $^{13}CO_2$-purged sample was multiplied by a factor of 4 for better comparison (see experimental details in the Supporting Information).

minimum at the cavity center. CO_2 was found to bind with two possible conformations in the pocket (second local minima found at $z = \pm 3.1$ Å). A snapshot of the final state after 22 ns of a MD simulation in $KHCO_3$ (0.1 M) is shown in Figure 3b. The CO molecule was initially placed in the cavity center and was found to be eventually replaced by two CO_2 molecules at the given concentration. The free-energy profiles were used to

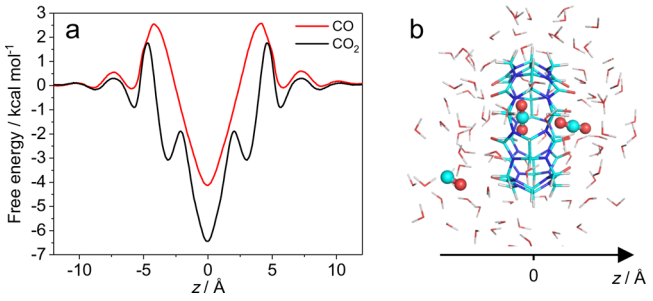

Figure 3. CO_2 and CO inclusion in CB[6] in 0.1 M $KHCO_3$ studied by MD simulations. (a) Free-energy profile of CO_2 and CO passing through the cavity of CB[6] along a central axis (the z axis is illustrated in (b) based on umbrella sampling of MD simulations). (b) Snapshot of MD simulation with one "deep cavity"-bound CO_2, one CO_2 loosely associated with carbonyl ring, and one unbound CO.

calculate the binding constants $K_{a,CO2}$ = 105 M^{-1} and $K_{a,CO}$ = 5 M^{-1} for CB[6]·CO_2 and CB[6]·CO, respectively (binding free-energies of 6.4 and 4.1 kcal mol^{-1}, respectively, see the Supporting Information for computational details).

To quantify the binding of CO_2 and CB[6] experimentally, fluorescent dye displacement measurements were performed (Figure 4a and Figure S6). This technique utilizes the fluorescence of the host–guest complex of CB[6] with an indicator dye, in this case *trans*-4[4-(dimethylamino)styryl]-1-methylpyridinium (DSMI, inset of Figure 4a). DSMI is weakly fluorescent on its own but strongly fluorescent in the complexed state.[41] The competitive binding of CO_2 and DSMI to the CB[6] cavity (Figure 4b) was used to determine a binding constant ($K_{a,CO2}$) of 250 ± 100 M^{-1} in 0.1 M $KHCO_3$ for the CB[6]·CO_2 host–guest complex. The experimental finding was qualitatively confirmed with a second indicator dye (Figure S6). This sizable affinity is in good agreement with the computational data. Unfortunately, CO afforded only a small change in fluorescence owing to its low solubility, which prevented an accurate quantification of its binding constant. However, well-established trends of gas affinities and corresponding volume/packing coefficients[31] along with the performed DFT and MD calculations suggest a weaker binding of CO than that of CO_2 to CB[6]. These findings indicate that there is no product inhibition (i.e., CO occupying the CB[6] pocket due to a higher binding affinity than that of CO_2), which is a general concern in (supramolecular) catalysis.[42]

Au Electrode Modification with CB[6]. The binding of CB[6] to Au surfaces has previously been reported[32,43] but rarely quantitatively. The effect of the solvent and the nature and concentration of the electrolyte were suspected to have a large effect on the surface adsorption equilibrium. Solubility of CB[6] in water is typically very low (<100 μM),[44] but it can be readily increased by more than 2 orders of magnitude through addition of cationic species to the solution.[45] Besides the increased solubility, the interaction of cations with CB[6] influences the kinetics of host–guest complex formation.[46] As an additional complexity, cations themselves have shown to effect CO_2 reduction on heterogeneous electrocatalysts.[47−50] Considering these multiple intricate effects of cations in the system, we employed an aqueous $KHCO_3$ (0.1 M) electrolyte solution, which is also commonly used in CO_2 reduction catalysis.[51,52] This concentration fulfills the necessity for supporting electrolytes during electrocatalytic CO_2 reduction and overcomes the limited solubility of CB[6] while

DOI: 10.1021/acscatal.9b04221
ACS Catal. 2020, 10, 751−761

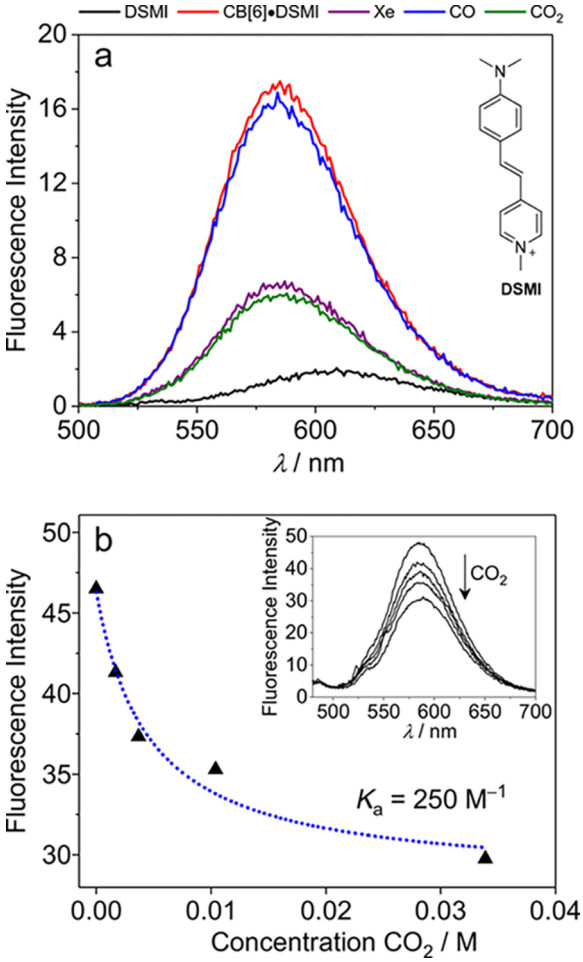

Figure 4. Fluorescent dye displacement measurements. (a) Fluorescence intensity of CB-free DSMI and the CB[6]·DSMI complex with and without competitive guests. The solution was saturated with the respective gas. Xe was used as a control with a known binding affinity. The DSMI counterion (iodide) was removed for clarity. (b) Decrease in fluorescence intensity of the CB[6]·DSMI complex with increasing CO_2 concentration to calculate the binding affinity of CO_2·CB[6] based on the known binding affinity of DSMI. The concentration of CO_2 was determined via Henry's law (see the Supporting Information for details). Experimental conditions: 0.1 M $KHCO_3$, [dye] = 1 μM, [CB[6]] = 50 μM, excitation wavelength = 283 nm, and $K_{a,DSMI}$ determined as 2100 M^{-1} in 0.1 M $KHCO_3$ (Figure S6).

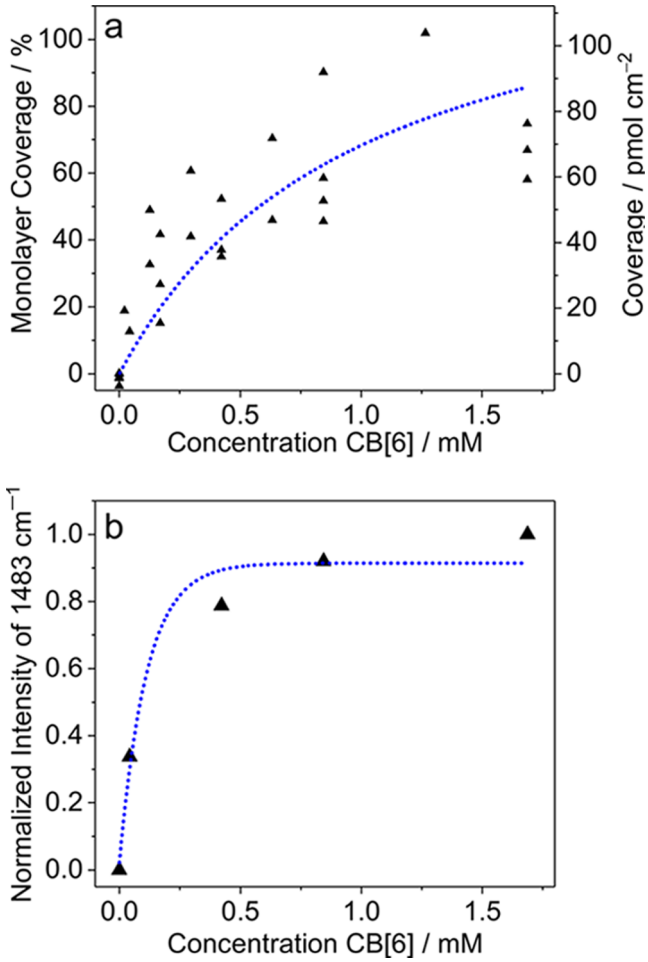

Figure 5. Surface adsorption of CB[6] on Au. (a) Monolayer coverage of CB[6] on Au-based on quartz-crystal microbalance measurements at an open-circuit potential. The data was modeled with the Sauerbrey equation and fitted with a Langmuir isotherm (blue dashed line). (b) Increase in relative intensity of the CB[6] band at 1483 cm^{-1} in SEIRA measurements and an exponential fit to guide the eye (blue dashed line).

minimizing the effects of cations on the host–guest complexation as well as on CO_2 reduction to a minimum.

The adsorption of CB[6] on Au was first quantified by quartz-crystal microbalance (QCM) measurements at open-circuit potential in N_2-purged $KHCO_3$ as shown in Figure 5a. The coverage was estimated using the Sauerbrey model,[53] assuming a flat gold surface and a van der Waals radius of "rigid" CB[6] of 14.4 Å.[45] A theoretical monolayer coverage of ca. 80 ± 20% for 1.69 mM CB[6] was determined with a Langmuir isotherm. Considering the highest density of hexagonally packed circles within a plane (ca. 90%), the data obtained from QCM is close to that for an optimally covered surface.

QCM was not only applied to study surface adsorption processes by mass changes but also further utilized to obtain insights into the viscoelasticity of the adsorbed layer by studying its dissipation behavior.[54] This can be particularly useful to gather information on changes of layer packing or, importantly, multilayer formation.[55,56] Measurements indicated that, for concentrations of >0.8 mM, the dissipation starts to increase, suggesting the formation of multilayers of CB[6] (Figure S7). Multilayer buildup of CB[6] on surfaces has been observed previously for CB[6] in solutions containing Na^+.[57] Furthermore, formation of chain-like coordination polymers between CB[6] and K^+ has been reported in the solid state.[58,59]

The interaction of CB[6] with the Au surface was further probed by SEIRA spectroscopy, which selectively monitors the Au–electrolyte interface (see below).[60,61] The vibrational band pattern of CB[6] revealed significantly different relative intensities between SEIRA and transmission measurements due to surface selection rules, indicating a preferential binding geometry of CB[6] on the surface compared to the isotropic case in solution (Figure S8). A notable shift of the carbonyl stretching mode from 1743 cm^{-1} in solution to 1737 cm^{-1} on the Au surface further suggests an interaction between (one of) the carbonyl-lined portals of CB[6] with the gold surface, which is in line with previous reports.[32,43,62] Figure 5b shows the normalized intensity of the intense 1483 cm^{-1} marker band

DOI: 10.1021/acscatal.9b04221
ACS Catal. 2020, 10, 751–761

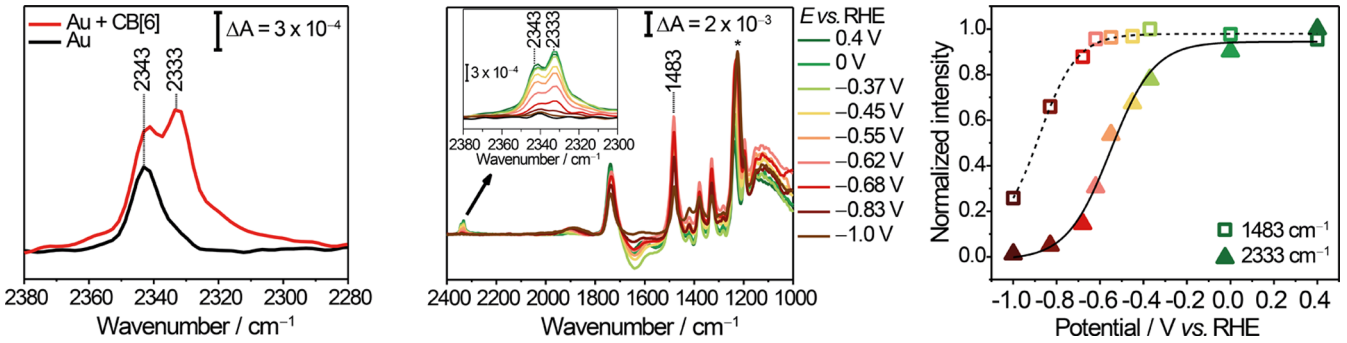

Figure 6. SEIRA measurements of CB[6]·CO_2 on Au. (a) SEIRA spectra of CO_2-purged 0.1 M $KHCO_3$ (black) and 1.69 mM CB[6] in 0.1 M $KHCO_3$ (red). Reference spectra: unmodified Au in argon-purged 0.1 M $KHCO_3$. (b) Potential dependent SEIRA spectra showing stepwise desorption of CB[6] from the surface at potentials more negative than −0.7 V vs RHE. Inset: the CB[6]·CO_2 band at 2333 cm^{-1} decreases rapidly at CO_2 reduction turnover potentials. Reference spectra: unmodified Au in argon-purged 0.1 M $KHCO_3$ at respective potentials. A spectral artifact (due to SiO_2 from the prism) at 1239 cm^{-1} marked with a star was found to have increased. (c) Normalized (between maximum and 0) intensity decline of band at 2333 and 1483 cm^{-1} with sigmoidal fits. Conditions: 1.69 mM CB[6] in 0.1 M $KHCO_3$. All potentials were *iR*-corrected (see the Supporting Information for details).

of CB[6] as a function of the CB[6] concentration in solution. No notable increase was observed for concentrations higher than ca. 1.3 mM (Figure S9), matching the concentration at which multilayer formation was observed in QCM measurements (Figure S7). As the SEIRA intensity I decreases significantly with distance d from the electrode surface ($I \approx d^{-6}$), potential multilayers of CB[6] cannot be monitored.[63] SEIRA as well as X-ray photoelectron spectroscopy (XPS) indicated a stable surface-bound CB[6] layer after overnight soaking in a CB[6]-free 0.1 M $KHCO_3$ aqueous electrolyte solution (Figures S10 and S11).

SEIRA Measurements of CB[6]·CO_2 under Polarization. SEIRA spectroscopy has recently gained increased attention in the field of CO_2 reduction catalysis due to its high sensitivity for surface processes.[64−67] Typically, the strong IR activity of CO and HCO_3^-/CO_3^{2-} is exploited to track specific bands to monitor product stability and binding, the bicarbonate/CO_2 equilibrium, and the role of cations. In this study, we specifically focus on the role of CO_2 and its fate upon inclusion into CB[6] during electrocatalytic turnover (see Figure 6).

Upon purging the electrolyte solution containing 1.69 mM CB[6] with CO_2, the band at 2333 cm^{-1} assigned to CB[6]·CO_2 appeared, indicating that CO_2 can efficiently penetrate the CB[6] cavity when the host molecule is bound to the Au surface. Compared to the isotropic case in the solution, the CB[6]·CO_2 band showed an increased intensity in the SEIRA spectra (Figure 6a) relative to the unaltered $CO_{2(aq)}$ band at 2343 cm^{-1}, suggesting an increase in the total CO_2 concentration (i.e., free $CO_{2(aq)}$ and CB[6]·CO_2) at the Au−electrolyte interface. We speculate that the binding of CB[6] to the Au surface together with its ability to host CO_2 acts as a driving force for CO_2 accumulation at the electrode surface.

SEIRA spectroscopic experiments in a three-electrode configuration were performed to investigate the behavior of the supramolecular complex on the surface at reductive potentials. To the best of our knowledge, the nature of the interaction as well as the stability of CB[6] on Au under electrochemical polarization have not yet been assessed in the literature. SEIRA spectra recorded at various potentials revealed that CB[6] starts to reversibly desorb from the electrode at −0.7 V versus the reversible hydrogen electrode (RHE; Figure 6). This is further confirmed by ex situ XPS measurements (Figure S12). Note that the anchoring of the carbonyl-lined portal of CB[6] is significantly different to chemisorption through commonly employed thiol groups on Au that suffer from low electrochemical stability under reductive conditions.[68] Though several groups have recently reported that multidentate thiol-anchoring provides improved stability of cocatalysts for CO_2 reduction, reductive desorption effects were not discussed in detail.[18,19]

As shown in Figure 6b,c, the intensity of the CB[6]·CO_2 band started to decline at potentials below ca. −0.4 V versus RHE, matching the catalytic onset for CO_2 reduction (see below). This observation indicates the reduction of CO_2 inside the Au-immobilized CB[6] cavity. Mere desorption of CB[6] hosting CO_2 at very reducing conditions, which would also cause a decay of the 2333 cm^{-1} band, can be excluded because the observed SEIRA signals of CB[6] remain constant at potentials that already afford a significant decrease of the CB[6]·CO_2 band (Figure 6c). Therefore, the results suggest that the effects of CB[6] host−guest chemistry can be exploited for CO_2 reduction at least at the desirable low overpotential region between −0.4 and −0.7 V versus RHE. Furthermore, the data imply that a part of the remaining surface-bound CB[6] has an empty cavity at potentials more negative than −0.8 V versus RHE.

Plotting the 2343 cm^{-1} band observed on unmodified Au surfaces and in the presence of CB[6] yielded matching trends suggesting that CO_2 reduction of "free" CO_2 proceeds in both cases in a similar environment (Figure S13). A potential shift of the 2333 cm^{-1} intensity curve by approximately 40 mV at potential values affording turnover was noted, which may be related to an altered CO_2 reduction reaction within the cavity. CB[6]-bound CO was not detected as expected from the low binding affinity and solubility of CO. Moreover, CB[6] marker bands in the CO_2-purged electrolyte were found to match those in Ar-purged solutions (Figure S14) also at very negative potentials. This indicates that the structure and conformation of CB[6] is maintained throughout the large potential window and under CO_2 binding, suggesting that there is no change in CO_2 binding affinity particularly at negative potentials.

Electrocatalysis. Stepped constant-potential electrolysis experiments were performed to monitor the influence of CB[6] on the activity and selectivity of CO_2 reduction on Au. The cell design with online gas sampling was based on recent

DOI: 10.1021/acscatal.9b04221
ACS Catal. 2020, 10, 751−761

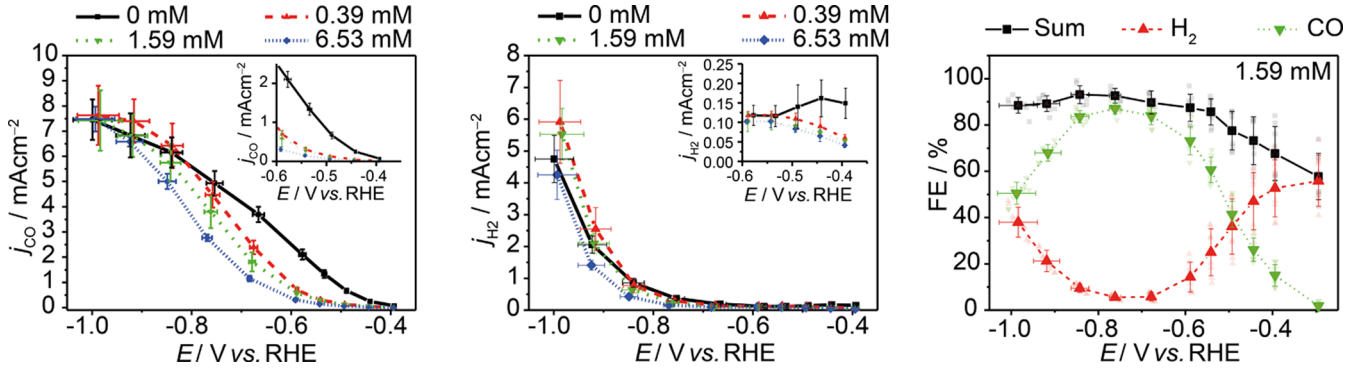

Figure 7. Constant-potential electrolysis at seven potentials with online gas quantification. The data represents averages and standard deviations of at least three independent stepped-chronoamperometry experiments. The x axis error is calculated based on a ±3 Ω change in uncompensated resistance. (a) Partial CO current density (j_{co}), (b) partial H_2 current density (j_{H2}), and (c) Faradaic efficiency of 1.59 mM CB[6] measurements.

reports[69,70] and is described in detail in the Supporting Information (Figures S15−S17). Additional characterization including diffusion layer thickness and electrochemical surface area determination following a recent report for more standardized data acquisition[71] is also reported in the Supporting Information (Figures S18−S20). The system showed good stability for 12 h (Figure S21). Figure 7 compares partial current densities at various potentials of Au electrodes in solutions of CB[6] of varying concentrations to cover the CB[6] monolayer and multilayer regimes. The results of unmodified (blank) Au agree with recently published findings.[7] Self-assembly of CB[6] prior to catalysis without CB[6] in the electrolyte solution during electrocatalysis showed marginal differences compared to unfunctionalized Au electrodes (Figure S22), which is presumably due to a less favorable adsorption equilibrium of CB[6] at negative applied potentials over the timespan of the electrocatalysis experiments.

In contrast, the presence of CB[6] in the solution was found to selectively alter the CO partial current density (j_{co}), while the hydrogen evolution current (j_{H2}) remained almost unchanged (Figure 7). In the potential window from −0.4 to −0.8 V versus RHE, j_{co} curves were observed to shift to more negative potentials with increasing CB[6] concentrations, corresponding to a suppression of j_{co} with CB[6] in the solution (Figure 7a; further details of electrocatalysis data in Figures S23−S27). At 0.39 mM CB[6], an approximately 100 mV more negative potential was required to achieve a comparable j_{co} than in the absence of CB[6]. No signals of CB[6] degradation were observed by nuclear magnetic resonance (NMR) spectroscopy (Figure S28), and $^{13}CO_2$ electrocatalysis experiments yielded exclusively ^{13}CO (Figure S29). Upon decreasing the potential to be more negative than −0.8 V versus RHE, a convergence of the j_{CO} in the absence and presence of CB[6] with different concentrations was observed (Figure 7a). This observation can be rationalized by the potential-induced desorption of CB[6] from the surface starting to occur at potentials more negative than −0.7 V versus RHE (Figure 6c).

Mechanistic Interpretation. The experimental data demonstrate that the electrocatalytic reduction of CO_2 on Au has been effectively altered by CB[6] encapsulation. This effect can be explained on a molecular basis through the macrocycle's impact particularly on the rate-determining step (RDS) of the catalytic process. In this respect, an initial electron transfer to CO_2 to form a Au−COO^- species and a proton-coupled electron transfer to form directly a Au−COOH species are often discussed as possible candidates.[4,64,72−74] Both cases would yield a Tafel slope of 118 mV dec^{-1} based on the initial electron transfer as the rate-limiting step, which matches our Tafel slopes of approximately 120 mV dec^{-1} for unmodified and CB[6]-coated Au surfaces (Figure S30). Thus, the unaffected Tafel slopes in the presence of CB[6] as well as the fact that only CO is generated allow us to draw the conclusion that the macrocycle-mediated catalytic CO_2 reduction likely proceeds via the same elementary steps as on bare Au. The altered catalytic performance however suggests that the new reaction environment induced by CB[6] has significantly altered the kinetics of relevant reaction steps. This can be rationalized by an altered energy landscape for the reaction through specific interactions on CO_2 and *COO^- within CB[6] compared to the blank Au interface. This is provided by the following qualitative arguments:

(1) The hydrophobic nature of the cavity lowers the availability of water molecules to stabilize surface-bound intermediates through hydrogen bond formation. Previous molecular dynamics simulations suggest approximately 3−4 water molecules in the cavity of solubilized CB[6] without a guest in the aqueous environment.[75] In line with this report, our MD simulations show that an average of less than one (0.62) water molecule is present within the space defined by the CB[6] carbonyl oxygen rims when CO_2 or CO is adsorbed in the CB[6] cavity.

(2) Cations such as K^+ have previously been shown to have a large effect on the CO_2 reduction reaction by stabilizing intermediates exhibiting a permanent dipole moment.[30] However, MD simulations show that the inclusion of K^+ into CB[6] is energetically unfavorable (Figure S3), and DFT-optimized structures of CB[6] with K^+ on a Au surface suggest that the distance between K^+ and the encapsulated surface-bound intermediate COOH is too large for a stabilizing interaction (Figure 8).

(3) Without further modifications, CB is known to stabilize electron-deficient guests via hydrophobic interactions in the cavity and electrostatic interactions at the carbonyl rim. Hence, direct stabilization of a charged intermediate by the CB[6] cavity is likely not being provided.[26]

(4) DFT and MD calculations presented above revealed an approximately 7 kcal mol^{-1} free-energy difference of CO_2 in CB[6] compared to being freely diffusing in

DOI: 10.1021/acscatal.9b04221
ACS Catal. 2020, 10, 751−761

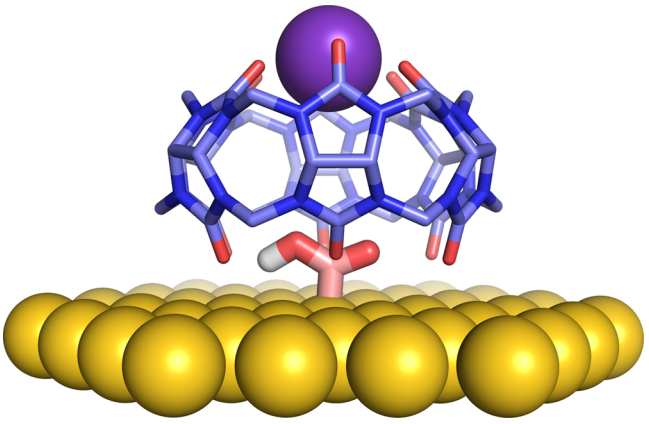

Figure 8. DFT calculation-derived model of the Au−COOH intermediate in the CB[6] cavity on the Au surface. K^+ is coordinated to the carbonyl lined rim of CB[6]. Color coding: purple: K^+, red: O, yellow: Au, light blue: C (CB [6]), dark blue: N, white: H (not shown for CB[6] for increased clarity), and light red: surface-bound C.

solution (Figure 3 and Table S1). This indicates that CO_2 is stabilized within CB[6] and thus exhibits a reduced capability for subsequent reactions without additional stabilization of the reaction intermediate.

The altered environment within CB[6] will eventually affect the thermodynamics and kinetics of formation of encapsulated surface-bound species. To gauge such effects, DFT calculations were performed particularly for the Au−COOH species formation (details in the Supporting Information, Figures S31 and S32). Calculations for Au−COO^- were not possible due the high level of complexity regarding the uncompensated charge. For CO_2, the results show a horizontally aligned molecule in the vicinity of the bare Au surface (Figure S32), whereas a more perpendicular orientation was found within CB[6], suggesting that inclusion affords a different stabilization of the substrate near the electrode surface.

Next, the reaction free-energy difference ($\Delta\Delta_R G$) of the reaction from Au−CO_2 to Au−COOH within CB[6] and at the blank Au surface was calculated. An increase of ∼8 kcal mol^{-1} (0.36 eV) was determined for the reaction proceeding in CB[6] compared to blank Au (Table S2). Thus, the calculation provides evidence for a notably increased energy required for the reaction upon encapsulation, which is proposed to result from the absence of solvent/cation-mediated stabilization of the product, that is, Au−COOH as discussed qualitatively above as well as from additional stabilization of the substrate CO_2 within CB[6]. This effect is expected to be even more pronounced when considering Au−COO^-, which should be energetically higher due to the absent charge compensation by the proton as well as the lack of other electrostatic interactions in the cavity as discussed above.

As a result, a higher-energy RDS is expected, leading to an overall decrease in j_{CO} (at the same applied potential) and therefore providing a molecular basis for explaining the increased overpotential required to reduce CO_2 inside the CB[6] cavity. In agreement, at a 0.39 mM CB[6] concentration corresponding to a quasi-monolayer of CB[6] on Au, an indicative shift in j_{co} of the CB[6]-modified electrode by ∼100 mV as aforementioned was observed. In this context, increasing the CB[6] concentration to 1.59 mM has little effect as the surface coverage is not significantly increased as demonstrated by QCM and SEIRA measurements (Figure 5). However, at 6.53 mM CB[6] where multilayer formation occurs, further, stronger suppression of the CO current density is apparent. Thus, for high CB[6] concentrations, j_{CO} is likely governed by additional factors, such as a hindered CO_2 uptake into CB[6] and CO release due to the adsorbed multilayers corresponding to an effective blocking of the electrode surface.

Host−Guest Design Criteria for Electrocatalysis. The rational manipulation of the heterogeneous interfacial catalytic process by creating well-defined reaction environments opens up promising avenues to selectively alter the catalytic transformation to desired outcomes in the future. Based on our findings, we propose three design criteria to rationally achieve an improved molecular cocatalyst system for CO_2 reduction to CO:

(1) The induced reaction environment should be modulated to selectively stabilize the surface-bound intermediate COO^-/COOH to help break scaling relationships.[9] Recent publications discuss the ability of amines[76] and amides[18,19,77] in a ligand construct as well as imidazolium-based ionic liquids[78,79] to stabilize CO_2 reduction intermediates via hydrogen bonding and/or electrostatic interactions on bare electrodes. In this respect, we envision that secondary guests within the CB cavity might be used to accommodate specific functional groups to selectively tune the active site environment. The larger CB[8] is able to incorporate two molecules within its cavity, which offers a large degree of tunability of the electrostatic and chemical environment within the cavity.[26]

(2) The inclusion of the substrate CO_2 should facilitate consecutive reactions, for example, by enabling specific interactions of CO_2 with the cavity analogous to enzyme active sites. We observed a 10 cm^{-1} shift toward lower wavenumbers for CO_2 inside the CB[6] cavity. This may suggest a decreased bond order of CO_2. Nevertheless, this effect might not be dominant in the presented system due to the lack of stabilization of a key intermediate (COOH/COO^-). The probing of interactions of CO_2 with a secondary guest in the CB cavity via vibrational spectroscopy might enable systematic studies of host·substrate binding prior to catalytic turnover.

(3) The kinetics of CO_2 uptake and CO release needs to be sufficiently fast to accomplish highly catalytic activities. A simple model calculation (see the Supporting Information) suggests that ingress and egress kinetics of CO_2 and CO, respectively, should be higher than 20 s^{-1} to obtain >5 mA cm^{-2} for j_{CO}. A high binding constant for CO_2 and low binding constant for CO should be maintained. The binding constant is defined as the ratio of ingress and egress kinetics,[46] and the egress kinetics for CO_2 and ingress kinetics for CO should therefore be slow. While enzymes have perfected this independent tuning of complexation kinetics and thermodynamics, it remains difficult to realize this in synthetic systems. The use of cations as "lids" for the CB portals has been suggested to influence host−guest complex formation kinetics.[45] This might enable a pathway through a variation of cations in the electrolyte solution to specifically alter the kinetics of substrate inclusion or product release. Moreover, addition of competitively binding non-redox-active guests could

DOI: 10.1021/acscatal.9b04221
ACS Catal. 2020, 10, 751−761

allow for further rational tuning of CO_2 ingress/egress kinetics by subtly changing the host−guest equilibria as well as electronics and sterics.

The manifold of new pathways to pursue shows that the CB[*n*]−Au hybrid system provides us with proposed measures and a modular platform to selectively tune different reaction steps of the heterogeneous CO_2 reduction at Au surfaces and to mechanistically explore electrocatalysis at the inorganic−organic interfaces. This allows for detailed investigations of the reaction mechanism by rational experimental design toward a complete understanding of the process. Such knowledge is a major prerequisite for the development of next generation electrocatalysts.

CONCLUSIONS

We present the concept of surface-adsorbed supramolecular host−guest chemistry in heterogeneous electrocatalysis. The combined spectroscopic, analytical, and electrocatalytic results suggest that CO_2 is captured within the cavity of the supramolecular host-molecule CB[6] and electrocatalytically reduced inside the cavity when adsorbed on the gold surface. An increased concentration of CO_2 is observed at the electrode−electrolyte interface due to the binding of CB[6]·CO_2.

The confinement of CO_2 reduction into CB[6] nanocavities enables molecular tunablity of the local chemical environment on the electrocatalyst surface. The presented data indicates that the CB[6] complexation strongly and selectively affects the electrocatalytic reduction of CO_2 to CO, while the hydrogen evolution activity remains essentially unchanged. The resultant hybrid organic−inorganic composite can thus be regarded as a model system for synthetic cavity-based heterogeneous electrocatalysts. Notably, a plethora of different research fields spanning from metal−organic frameworks[80,81] and covalent−organic frameworks[82] to molecular catalysis[83−86] and synthetic biology[87] are also heavily focused on tuning the local environment and coordination spheres around a catalytic active site. The development of such model systems and analytical methodology as presented here may help us to gain insight in this complex and important field of research. In the context of CO_2 reduction electrocatalysis, this may offer new routes to overcome scaling relationships and rationally tune the selectivity and activity of electrodes also beyond Au. Thus, this concept bridges the gap between enzymatic, molecular, and heterogeneous catalysis and may open up new avenues for utilizing fine-tuned supramolecular units as synthetic catalytic pockets.

ASSOCIATED CONTENT

Supporting Information

The Supporting Information is available free of charge at https://pubs.acs.org/doi/10.1021/acscatal.9b04221.

Detailed experimental procedures, additional transmission IR, SEIRA, QCM, XPS, MD, DFT, fluorescence, electrochemical characterization and electrocatalysis results (PDF)

AUTHOR INFORMATION

Corresponding Authors

*E-mail: oas23@cam.ac.uk (O.A.S.).
*E-mail: reisner@ch.cam.ac.uk (E.R.).

ORCID

Andreas Wagner: 0000-0003-4464-4345
István Szabó: 0000-0002-3700-3614
Khaleel I. Assaf: 0000-0003-4331-8492
Steven J. Barrow: 0000-0001-6417-1800
Mohamed Al-Hada: 0000-0002-2913-9490
Nikolay Kornienko: 0000-0001-7193-2428
Moritz F. Kuehnel: 0000-0001-8678-3779
Edina Rosta: 0000-0002-9823-4766
Ingo Zebger: 0000-0002-6354-3585
Werner M. Nau: 0000-0002-7654-6232
Oren A. Scherman: 0000-0001-8032-7166
Erwin Reisner: 0000-0002-7781-1616

Present Addresses

◆K.H.L.: Fakultät für Chemie und Lebensmittelchemie, Technische Universität Dresden, 01062 Dresden, Germany.
●M.F.K.: Department of Chemistry, Swansea University, College of Science, Singleton Park, Swansea SA2 8PP, U.K.
□K.I.A.: Department of Chemistry, Al-Balqa Applied University, Al-Salt 19117, Jordan
&S.J.B.: School of Applied Chemistry and Environmental Science, RMIT University, Melbourne, 3000, Victoria, Australia.
¶N.K. and N.H.: Department of Chemistry, Université de Montréal, Roger-Gaudry Building, Montreal, Quebec, H3C 3J7, Canada.

Author Contributions

○A.W. and K.H.L. contributed equally to this work.

Notes

The authors declare no competing financial interest.
Additional data related to this publication are available at the University of Cambridge data repository (https://doi.org/10.17863/CAM.46170).

ACKNOWLEDGMENTS

We gratefully acknowledge financial support from the Christian Doppler Research Association, Austrian Federal Ministry for Digital and Economic Affairs, National Foundation for Research, Technology and Development, OMV Group (to A.W., M.F.K., and Er.R.), EU ERC Consolidator grant "MatEnSAP" (no. 68283 to N.H. and Er.R.) and Starting Grant "BioNet" (no. 757850 to Ed.R.), Royal Society Newton International Fellowship (no. NF160054 to N.K.), European Commission for Marie Curie Fellowships (NANOSPHERE, no. 658360 to S.J.B.; VSHER, no. 701192 to K.H.L.; and ESTIMABLeNANO, no. 706425 to K.S.), EPSRC (nos. EP/R013012/1 and EP/N020669/1 to Ed.R. and no. EP/L027151/1 for O.A.S.), and DFG, Deutsche Forschungsgemeinschaft/German Research Foundation (to K.I.A. and W.M.N.) as well as funding under Germany's Excellence Strategy − EXC 2008/1 − 390540038 (UniSysCat) (i.a. to I.Z.). We are also grateful to the U.K. Materials and Molecular Modelling Hub for computational resources, which is partially funded by EPSRC (no. EP/P020194/1). We would like to thank Mr. Simon Dowe for the help in the design and manufacturing of the electrochemical cell, Dr. Guanglu Wu and Dr. Annika Eisenschmidt for their help with NMR spectroscopy, Dr. Jade Alexis McCune for a CB[6] sample, and Mr. Dénes Berta for discussion regarding DFT computations.

DOI: 10.1021/acscatal.9b04221
ACS Catal. 2020, 10, 751−761

REFERENCES

(1) Qiao, J.; Liu, Y.; Hong, F.; Zhang, J. A Review of Catalysts for the Electroreduction of Carbon Dioxide to Produce Low-Carbon Fuels. *Chem. Soc. Rev.* **2014**, *43*, 631−675.

(2) Lewis, N. S.; Nocera, D. G. Powering the Planet: Chemical Challenges in Solar Energy Utilization. *Proc. Natl. Acad. Sci. USA* **2006**, *103*, 15729−15735.

(3) Whipple, D. T.; Kenis, P. J. A. Prospects of CO_2 Utilization via Direct Heterogeneous Electrochemical Reduction. *J. Phys. Chem. Lett.* **2010**, *1*, 3451−3458.

(4) Kortlever, R.; Shen, J.; Schouten, K. J. P.; Calle-Vallejo, F.; Koper, M. T. M. Catalysts and Reaction Pathways for the Electrochemical Reduction of Carbon Dioxide. *J. Phys. Chem. Lett.* **2015**, *6*, 4073−4082.

(5) Jhong, H.-R. M.; Ma, S.; Kenis, P. J. Electrochemical Conversion of CO_2 to Useful Chemicals: Current Status, Remaining Challenges, and Future Opportunities. *Curr. Opin. Chem. Eng.* **2013**, *2*, 191−199.

(6) Hori, Y.; Murata, A.; Kikuchi, K.; Suzuki, S. Electrochemical Reduction of Carbon Dioxide to Carbon Monoxide at a Gold Electrode in Aqueous Potassium Hydrogen Carbonate. *J. Chem. Soc., Chem. Commun.* **1987**, 728−729.

(7) Cave, E. R.; Montoya, J. H.; Kuhl, K. P.; Abram, D. N.; Hatsukade, T.; Shi, C.; Hahn, C.; Nørskov, J. K.; Jaramillo, T. F. Electrochemical CO_2 Reduction on Au Surfaces: Mechanistic Aspects Regarding the Formation of Major and Minor Products. *Phys. Chem. Chem. Phys.* **2017**, *19*, 15856−15863.

(8) Chen, Y.; Li, C. W.; Kanan, M. W. Aqueous CO_2 Reduction at Very Low Overpotential on Oxide-Derived Au Nanoparticles. *J. Am. Chem. Soc.* **2012**, *134*, 19969−19972.

(9) Hansen, H. A.; Varley, J. B.; Peterson, A. A.; Nørskov, J. K. Understanding Trends in the Electrocatalytic Activity of Metals and Enzymes for CO_2 Reduction to CO. *J. Phys. Chem. Lett.* **2013**, *4*, 388−392.

(10) Zhu, W.; Zhang, Y.-J.; Zhang, H.; Lv, H.; Li, Q.; Michalsky, R.; Peterson, A. A.; Sun, S. Active and Selective Conversion of CO_2 to CO on Ultrathin Au Nanowires. *J. Am. Chem. Soc.* **2014**, *136*, 16132−16135.

(11) Shi, C.; Hansen, H. A.; Lausche, A. C.; Nørskov, J. K. Trends in Electrochemical CO_2 Reduction Activity for Open and Close-Packed Metal Surfaces. *Phys. Chem. Chem. Phys.* **2014**, *16*, 4720−4727.

(12) Li, Y.; Sun, Q. Recent Advances in Breaking Scaling Relations for Effective Electrochemical Conversion of CO_2. *Adv. Energy Mater.* **2016**, *6*, 1600463.

(13) Kim, D.; Resasco, J.; Yu, Y.; Asiri, A. M.; Yang, P. Synergistic Geometric and Electronic Effects for Electrochemical Reduction of Carbon Dioxide Using Gold-Copper Bimetallic Nanoparticles. *Nat. Commun.* **2014**, *5*, 4948.

(14) Torelli, D. A.; Francis, S. A.; Crompton, J. C.; Javier, A.; Thompson, J. R.; Brunschwig, B. S.; Soriaga, M. P.; Lewis, N. S. Nickel−Gallium-Catalyzed Electrochemical Reduction of CO_2 to Highly Reduced Products at Low Overpotentials. *ACS Catal.* **2016**, *6*, 2100−2104.

(15) Calle-Vallejo, F.; Loffreda, D.; Koper, M. T. M.; Sautet, P. Introducing Structural Sensitivity into Adsorption−Energy Scaling Relations by Means of Coordination Numbers. *Nat. Chem.* **2015**, *7*, 403−410.

(16) Fang, Y.; Flake, J. C. Electrochemical Reduction of CO_2 at Functionalized Au Electrodes. *J. Am. Chem. Soc.* **2017**, *139*, 3399−3405.

(17) Xie, M. S.; Xia, B. Y.; Li, Y.; Yan, Y.; Yang, Y.; Sun, Q.; Chan, S. H.; Fisher, A.; Wang, X. Amino Acid Modified Copper Electrodes for the Enhanced Selective Electroreduction of Carbon Dioxide towards Hydrocarbons. *Energy Environ. Sci.* **2016**, *9*, 1687−1695.

(18) Gong, M.; Cao, Z.; Liu, W.; Nichols, E. M.; Smith, P. T.; Derrick, J. S.; Liu, Y.-S.; Liu, J.; Wen, X.; Chang, C. J. Supramolecular Porphyrin Cages Assembled at Molecular−Materials Interfaces for Electrocatalytic CO Reduction. *ACS Cent. Sci.* **2017**, *3*, 1032−1040.

(19) Cao, Z.; Zacate, S. B.; Sun, X.; Liu, J.; Hale, E. M.; Carson, W. P.; Tyndall, S. B.; Xu, J.; Liu, X.; Liu, X.; Song, C.; Luo, J.; Cheng, M.-J.; Wen, X.; Liu, W. Tuning Gold Nanoparticles with Chelating Ligands for Highly Efficient Electrocatalytic CO_2 Reduction. *Angew. Chem., Int. Ed.* **2018**, *57*, 12675−12679.

(20) Cao, Z.; Kim, D.; Hong, D.; Yu, Y.; Xu, J.; Lin, S.; Wen, X.; Nichols, E. M.; Jeong, K.; Reimer, J. A.; Yang, P.; Chang, C. J. A Molecular Surface Functionalization Approach to Tuning Nanoparticle Electrocatalysts for Carbon Dioxide Reduction. *J. Am. Chem. Soc.* **2016**, *138*, 8120−8125.

(21) Shin, W.; Lee, S. H.; Shin, J. W.; Lee, S. P.; Kim, Y. Highly Selective Electrocatalytic Conversion of CO_2 to CO at −0.57 V (NHE) by Carbon Monoxide Dehydrogenase from Moorella thermoacetica. *J. Am. Chem. Soc.* **2003**, *125*, 14688−14689.

(22) Parkin, A.; Seravalli, J.; Vincent, K. A.; Ragsdale, S. W.; Armstrong, F. A. Rapid and Efficient Electrocatalytic CO_2/CO Interconversions by Carboxydothermus Hydrogenoformans CO Dehydrogenase I on an Electrode. *J. Am. Chem. Soc.* **2007**, *129*, 10328−10329.

(23) Robinson, W. E.; Bassegoda, A.; Reisner, E.; Hirst, J. Oxidation-State-Dependent Binding Properties of the Active Site in a Mo-Containing Formate Dehydrogenase. *J. Am. Chem. Soc.* **2017**, *139*, 9927−9936.

(24) Shi, J.; Jiang, Y.; Jiang, Z.; Wang, X.; Wang, X.; Zhang, S.; Han, P.; Yang, C. Enzymatic Conversion of Carbon Dioxide. *Chem. Soc. Rev.* **2015**, *44*, 5981−6000.

(25) Can, M.; Armstrong, F. A.; Ragsdale, S. W. Structure, Function, and Mechanism of the Nickel Metalloenzymes, CO Dehydrogenase, and Acetyl-CoA Synthase. *Chem. Rev.* **2014**, *114*, 4149−4174.

(26) Barrow, S. J.; Kasera, S.; Rowland, M. J.; del Barrio, J.; Scherman, O. A. Cucurbituril-Based Molecular Recognition. *Chem. Rev.* **2015**, *115*, 12320−12406.

(27) You, H.; Wu, D.; Chen, Z.; Sun, F.; Zhang, H.; Chen, Z.; Cao, M.; Zhuang, W.; Cao, R. Highly Active and Stable Water Splitting in Acidic Media Using a Bifunctional Iridium/Cucurbit[6]uril Catalyst. *ACS Energy Lett.* **2019**, *4*, 1301−1307.

(28) Kaifer, A. E. Toward Reversible Control of Cucurbit[*n*]uril Complexes. *Acc. Chem. Res.* **2014**, *47*, 2160−2167.

(29) Mitkina, T. V.; Zakharchuk, N. F.; Naumov, D. Y.; Gerasko, O. A.; Fenske, D.; Fedin, V. P. Syntheses, Structures, and Electrochemical Properties of Inclusion Compounds of Cucurbit[8]uril with Cobalt(III) and Nickel(II) Complexes. *Inorg. Chem.* **2008**, *47*, 6748−6755.

(30) Assaf, K. I.; Nau, W. M. Cucurbiturils: From Synthesis to High-Affinity Binding and Catalysis. *Chem. Soc. Rev.* **2015**, *44*, 394−418.

(31) Florea, M.; Nau, W. M. Strong Binding of Hydrocarbons to Cucurbituril Probed by Fluorescent Dye Displacement: A Supramolecular Gas-Sensing Ensemble. *Angew. Chem., Int. Ed.* **2011**, *50*, 9338−9342.

(32) An, Q.; Li, G.; Tao, C.; Li, Y.; Wu, Y.; Zhang, W. A General and Efficient Method to Form Self-Assembled Cucurbit[*n*]uril Monolayers on Gold Surfaces. *Chem. Commun.* **2008**, *36*, 1989−1991.

(33) Shin, J. W.; Bertocci, U.; Stafford, G. R. Stress Response to Surface Alloying and Dealloying during Underpotential Deposition of Pb on (111)-Textured Au. *J. Phys. Chem. C* **2010**, *114*, 7926−7932.

(34) Rojas, M. T.; Königer, R.; Stoddart, J. F.; Kaifer, A. E. Supported Monolayers Containing Preformed Binding Sites. Synthesis and Interfacial Binding Properties of a Thiolated *β*-Cyclodextrin Derivative. *J. Am. Chem. Soc.* **1995**, *117*, 336−343.

(35) Yao, Y.; Xue, M.; Zhang, Z.; Zhang, M.; Wang, Y.; Huang, F. Gold Nanoparticles Stabilized by an Amphiphilic Pillar[5]Arene: Preparation, Self-Assembly into Composite Microtubes in Water and Application in Green Catalysis. *Chem. Sci.* **2013**, *4*, 3667.

(36) Kim, H.; Kim, Y.; Yoon, M.; Lim, S.; Park, S. M.; Seo, G.; Kim, K. Highly Selective Carbon Dioxide Sorption in an Organic Molecular Porous Material. *J. Am. Chem. Soc.* **2010**, *132*, 12200−12202.

(37) Mohan, M.; Suzuki, T.; Nair, A. K.; Pillai, S.; Warrier, K. G. K.; Hareesh, U. S.; Nair, B. N.; Gale, J. D. Surface Modification Induced Enhanced CO_2 Sorption in Cucurbit[6]uril, an Organic Porous Material. *Phys. Chem. Chem. Phys.* **2017**, *19*, 25564−25573.

DOI: 10.1021/acscatal.9b04221
ACS Catal. 2020, 10, 751−761

(38) Falk, M.; Miller, A. G. Infrared Spectrum of Carbon Dioxide in Aqueous Solution. *Vib. Spectrosc.* **1992**, *4*, 105−108.
(39) Mock, W. L.; Shih, N. Y. Structure and Selectivity in Host-Guest Complexes of Cucurbituril. *J. Org. Chem.* **1986**, *51*, 4440−4446.
(40) Pan, S.; Saha, R.; Mandal, S.; Mondal, S.; Gupta, A.; Fernández-Herrera, M. A.; Merino, G.; Chattaraj, P. K. Selectivity in Gas Adsorption by Molecular Cucurbit[6]uril. *J. Phys. Chem. C* **2016**, *120*, 13911−13921.
(41) Ghale, G.; Nau, W. M. Dynamically Analyte-Responsive Macrocyclic Host−Fluorophore Systems. *Acc. Chem. Res.* **2014**, *47*, 2150−2159.
(42) Palma, A.; Artelsmair, M.; Wu, G.; Lu, X.; Barrow, S. J.; Uddin, N.; Rosta, E.; Masson, E.; Scherman, O. A. Cucurbit[7]uril as a Supramolecular Artificial Enzyme for Diels-Alder Reactions. *Angew. Chem., Int. Ed.* **2017**, *56*, 15688−15692.
(43) Lee, T.-C.; Scherman, O. A. Formation of Dynamic Aggregates in Water by Cucurbit[5]uril Capped with Gold Nanoparticles. *Chem. Commun.* **2010**, *46*, 2438−2440.
(44) McCune, J. A.; Kunz, S.; Olesińska, M.; Scherman, O. A. DESolution of CD and CB Macrocycles. *Chem. − Eur. J.* **2017**, *23*, 8601−8604.
(45) Jeon, Y.-M.; Kim, J.; Whang, D.; Kim, K. Molecular Container Assembly Capable of Controlling Binding and Release of Its Guest Molecules: Reversible Encapsulation of Organic Molecules in Sodium Ion Complexed Cucurbituril. *J. Am. Chem. Soc.* **1996**, *118*, 9790−9791.
(46) Márquez, C.; Hudgins, R. R.; Nau, W. M. Mechanism of Host−Guest Complexation by Cucurbituril. *J. Am. Chem. Soc.* **2004**, *126*, 5806−5816.
(47) Murata, A.; Hori, Y. Product Selectivity Affected by Cationic Species in Electrochemical Reduction of CO_2 and CO at a Cu Electrode. *Bull. Chem. Soc. Jpn* **1991**, *64*, 123−127.
(48) Kyriacou, G. Z.; Anagnostopoulos, A. K. Influence CO_2 Partial Pressure and the Supporting Electrolyte Cation on the Product Distribution in CO_2 Electroreduction. *J. Appl. Electrochem.* **1993**, *23*, 483−486.
(49) Thorson, M. R.; Siil, K. I.; Kenis, P. J. A. Effect of Cations on the Electrochemical Conversion of CO_2 to CO. *J. Electrochem. Soc.* **2012**, *160*, F69−F74.
(50) Resasco, J.; Chen, L. D.; Clark, E.; Tsai, C.; Hahn, C.; Jaramillo, T. F.; Chan, K.; Bell, A. T. Promoter Effects of Alkali Metal Cations on the Electrochemical Reduction of Carbon Dioxide. *J. Am. Chem. Soc.* **2017**, *139*, 11277−11287.
(51) Kuhl, K. P.; Hatsukade, T.; Cave, E. R.; Abram, D. N.; Kibsgaard, J.; Jaramillo, T. F. Electrocatalytic Conversion of Carbon Dioxide to Methane and Methanol on Transition Metal Surfaces. *J. Am. Chem. Soc.* **2014**, *136*, 14107−14113.
(52) Kim, D.; Kley, C. S.; Li, Y.; Yang, P. Copper Nanoparticle Ensembles for Selective Electroreduction of CO_2 to C_2 −C_3 Products. *Proc. Natl. Acad. Sci.* **2017**, *114*, 10560−10565.
(53) Sauerbrey, G. Verwendung von Schwingquarzen Zur Waegung Duenner Schichten Und Zur Mikrowaegung. *Z. Phys.* **1959**, *155*, 206−222.
(54) Singh, K.; Blanford, C. F. Electrochemical Quartz Crystal Microbalance with Dissipation Monitoring: A Technique to Optimize Enzyme Use in Bioelectrocatalysis. *ChemCatChem* **2014**, *6*, 921−929.
(55) Dixon, M. C. Quartz Crystal Microbalance with Dissipation Monitoring: Enabling Real-Time Characterization of Biological Materials and Their Interactions. *J. Biomol. Tech.* **2008**, *19*, 151−158.
(56) Notley, S. M.; Eriksson, M.; Wågberg, L. Visco-Elastic and Adhesive Properties of Adsorbed Polyelectrolyte Multilayers Determined in Situ with QCM-D and AFM Measurements. *J. Colloid Interface Sci.* **2005**, *292*, 29−37.
(57) Blanco, E.; Quintana, C.; Hernández, L.; Hernández, P. Atomic Force Microscopy Study of New Sensing Platforms: Cucurbit[*n*]uril (*n* =6, 7) on Gold. *Electroanalysis* **2013**, *25*, 263−268.
(58) Heo, J.; Kim, J.; Whang, D.; Kim, K. Columnar One-Dimensional Coordination Polymer Formed with a Metal Ion and a Host−Guest Complex as Building Blocks: Potassium Ion Complexed Cucurbituril. *Inorg. Chim. Acta* **2000**, *297*, 307−312.
(59) Ni, X.-L.; Xiao, X.; Cong, H.; Liang, L.-L.; Cheng, K.; Cheng, X.-J.; Ji, N.-N.; Zhu, Q.-J.; Xue, S.-F.; Tao, Z. Cucurbit[*n*]uril-Based Coordination Chemistry: From Simple Coordination Complexes to Novel Poly-Dimensional Coordination Polymers. *Chem. Soc. Rev.* **2013**, *42*, 9480.
(60) Osawa, M.; Ataka, K.-I.; Ikeda, M.; Uchihara, H.; Nanba, R. Surface Enhanced Infrared Absorption Spectroscopy. *Anal. Sci.* **1991**, *7*, 503−506.
(61) Wisitruangsakul, N.; Zebger, I.; Ly, K. H.; Murgida, D. H.; Ekgasit, S.; Hildebrandt, P. Redox-Linked Protein Dynamics of Cytochrome c Probed by Time-Resolved Surface Enhanced Infrared Absorption Spectroscopy. *Phys. Chem. Chem. Phys.* **2008**, *10*, 5276−5286.
(62) Chikkaraddy, R.; de Nijs, B.; Benz, F.; Barrow, S. J.; Scherman, O. A.; Rosta, E.; Demetriadou, A.; Fox, P.; Hess, O.; Baumberg, J. J. Single-Molecule Strong Coupling at Room Temperature in Plasmonic Nanocavities. *Nature* **2016**, *535*, 127−130.
(63) Osawa, M. Surface-Enhanced Infrared Absorption. In *Near-Field Optics and Surface Plasmon Polaritons*; Springer Berlin Heidelberg: Berlin, Heidelberg, 2001; pp 163−187.
(64) Wuttig, A.; Yaguchi, M.; Motobayashi, K.; Osawa, M.; Surendranath, Y. Inhibited Proton Transfer Enhances Au-Catalyzed CO_2-to-Fuels Selectivity. *Proc. Natl. Acad. Sci.* **2016**, *113*, E4585−E4593.
(65) Wuttig, A.; Liu, C.; Peng, Q.; Yaguchi, M.; Hendon, C. H.; Motobayashi, K.; Ye, S.; Osawa, M.; Surendranath, Y. Tracking a Common Surface-Bound Intermediate during CO_2-to-Fuels Catalysis. *ACS Cent. Sci.* **2016**, *2*, 522−528.
(66) Dunwell, M.; Lu, Q.; Heyes, J. M.; Rosen, J.; Chen, J. G.; Yan, Y.; Jiao, F.; Xu, B. The Central Role of Bicarbonate in the Electrochemical Reduction of Carbon Dioxide on Gold. *J. Am. Chem. Soc.* **2017**, *139*, 3774−3783.
(67) Heidary, N.; Ly, K. H.; Kornienko, N. Probing CO_2 Conversion Chemistry on Nanostructured Surfaces with Operando Vibrational Spectroscopy. *Nano Lett.* **2019**, *19*, 4817−4826.
(68) Love, J. C.; Estroff, L. A.; Kriebel, J. K.; Nuzzo, R. G.; Whitesides, G. M. Self-Assembled Monolayers of Thiolates on Metals as a Form of Nanotechnology. *Chem. Rev* **2005**, *105*, 1103−1170.
(69) Kuhl, K. P.; Cave, E. R.; Abram, D. N.; Jaramillo, T. F. New Insights into the Electrochemical Reduction of Carbon Dioxide on Metallic Copper Surfaces. *Energy Environ. Sci.* **2012**, *5*, 7050−7059.
(70) Lobaccaro, P.; Singh, M. R.; Clark, E. L.; Kwon, Y.; Bell, A. T.; Ager, J. W. Effects of Temperature and Gas−Liquid Mass Transfer on the Operation of Small Electrochemical Cells for the Quantitative Evaluation of CO_2 Reduction Electrocatalysts. *Phys. Chem. Chem. Phys.* **2016**, *18*, 26777−26785.
(71) Clark, E. L.; Resasco, J.; Landers, A.; Lin, J.; Chung, L.-T.; Walton, A.; Hahn, C.; Jaramillo, T. F.; Bell, A. T. Standards and Protocols for Data Acquisition and Reporting for Studies of the Electrochemical Reduction of Carbon Dioxide. *ACS Catal.* **2018**, *8*, 6560−6570.
(72) Wuttig, A.; Yoon, Y.; Ryu, J.; Surendranath, Y. Bicarbonate Is Not a General Acid in Au-Catalyzed CO_2 Electroreduction. *J. Am. Chem. Soc.* **2017**, *139*, 17109−17113.
(73) Dunwell, M.; Luc, W.; Yan, Y.; Jiao, F.; Xu, B. Understanding Surface-Mediated Electrochemical Reactions: CO_2 Reduction and Beyond. *ACS Catal.* **2018**, 8121−8129.
(74) Zhang, B. A.; Ozel, T.; Elias, J. S.; Costentin, C.; Nocera, D. G. Interplay of Homogeneous Reactions, Mass Transport, and Kinetics in Determining Selectivity of the Reduction of CO_2 on Gold Electrodes. *ACS Cent. Sci.* **2019**, *5*, 1097−1105.
(75) Biedermann, F.; Uzunova, V. D.; Scherman, O. A.; Nau, W. M.; De Simone, A. Release of High-Energy Water as an Essential Driving Force for the High-Affinity Binding of Cucurbit[*n*]urils. *J. Am. Chem. Soc.* **2012**, *134*, 15318−15323.
(76) Azcarate, I.; Costentin, C.; Robert, M.; Savéant, J.-M. Through-Space Charge Interaction Substituent Effects in Molecular Catalysis

DOI: 10.1021/acscatal.9b04221
ACS Catal. 2020, 10, 751−761

Leading to the Design of the Most Efficient Catalyst of CO_2-to-CO Electrochemical Conversion. *J. Am. Chem. Soc.* **2016**, *138*, 16639−16644.
(77) Nichols, E. M.; Derrick, J. S.; Nistanaki, S. K.; Smith, P. T.; Chang, C. J. Positional Effects of Second-Sphere Amide Pendants on Electrochemical CO_2 Reduction Catalyzed by Iron Porphyrins. *Chem. Sci.* **2018**, *9*, 2952−2960.
(78) Rosen, B. A.; Salehi-Khojin, A.; Thorson, M. R.; Zhu, W.; Whipple, D. T.; Kenis, P. J. A.; Masel, R. I. Ionic Liquid-Mediated Selective Conversion of CO_2 to CO at Low Overpotentials. *Science* **2011**, *334*, 643−644.
(79) Lau, G. P. S.; Schreier, M.; Vasilyev, D.; Scopelliti, R.; Grätzel, M.; Dyson, P. J. New Insights Into the Role of Imidazolium-Based Promoters for the Electroreduction of CO_2 on a Silver Electrode. *J. Am. Chem. Soc.* **2016**, *138*, 7820−7823.
(80) Hendon, C. H.; Rieth, A. J.; Korzyński, M. D.; Dincă, M. Grand Challenges and Future Opportunities for Metal-Organic Frameworks. *ACS Cent. Sci.* **2017**, *3*, 554−563.
(81) Hod, I.; Sampson, M. D.; Deria, P.; Kubiak, C. P.; Farha, O. K.; Hupp, J. T. Fe-Porphyrin-Based Metal−Organic Framework Films as High-Surface Concentration, Heterogeneous Catalysts for Electrochemical Reduction of CO_2. *ACS Catal.* **2015**, *5*, 6302−6309.
(82) Diercks, C. S.; Lin, S.; Kornienko, N.; Kapustin, E. A.; Nichols, E. M.; Zhu, C.; Zhao, Y.; Chang, C. J.; Yaghi, O. M. Reticular Electronic Tuning of Porphyrin Active Sites in Covalent Organic Frameworks for Electrocatalytic Carbon Dioxide Reduction. *J. Am. Chem. Soc.* **2018**, *140*, 1116−1122.
(83) Ginovska-Pangovska, B.; Dutta, A.; Reback, M. L.; Linehan, J. C.; Shaw, W. J. Beyond the Active Site: The Impact of the Outer Coordination Sphere on Electrocatalysts for Hydrogen Production and Oxidation. *Acc. Chem. Res.* **2014**, *47*, 2621−2630.
(84) Caserta, G.; Roy, S.; Atta, M.; Artero, V.; Fontecave, M. Artificial Hydrogenases: Biohybrid and Supramolecular Systems for Catalytic Hydrogen Production or Uptake. *Curr. Opin. Chem. Biol.* **2015**, *25*, 36−47.
(85) Reuillard, B.; Warnan, J.; Leung, J. J.; Wakerley, D. W.; Reisner, E. A Poly(Cobaloxime)/Carbon Nanotube Electrode: Freestanding Buckypaper with Polymer-Enhanced H_2-Evolution Performance. *Angew. Chem., Int. Ed.* **2016**, *55*, 3952−3957.
(86) Birdja, Y. Y.; Vos, R. E.; Wezendonk, T. A.; Jiang, L.; Kapteijn, F.; Koper, M. T. M. Effects of Substrate and Polymer Encapsulation on CO_2 Electroreduction by Immobilized Indium(III) Protoporphyrin. *ACS Catal.* **2018**, *8*, 4420−4428.
(87) Lancaster, L.; Abdallah, W.; Banta, S.; Wheeldon, I. Engineering Enzyme Microenvironments for Enhanced Biocatalysis. *Chem. Soc. Rev.* **2018**, *47*, 5177−5186.

DOI: 10.1021/acscatal.9b04221
ACS Catal. 2020, 10, 751−761